Co-existing fluid and silicate inclusions in mantle diamond

E.L. Tomlinson[1*], A.P. Jones[2], and J.W. Harris[3]

[1]Department of Geology, Royal Holloway University of London, Egham Hill
Egham, Surrey, TW20 0EX, U.K.
[2]Department of Earth Sciences, University College London, Gower Street, London WC1E 6BT, U.K.
[3]Division of Earth Sciences, University of Glasgow, The Gregory Building, Lilybank Gardens, Glasgow, G12 8QQ, U.K.

*e.tomlinson@gl.rhul.ac.uk

We have analysed the compositions of co-existing silicate macro-inclusions and fluid micro-inclusions in the fibrous coats of eight coated diamonds from the Panda kimberlite (Canada), by electron microprobe and infrared spectroscopy. The mineral inclusions in the diamond coats come from either the peridotite suite (Cr-pyrope, orthopyroxene, olivine and Cr-diopside) or eclogite suite (omphacite). Therefore, fibrous diamonds may grow in the same paragenetic environments as octahedral diamonds. The inclusions document a more fertile source composition (lower Mg# and higher Ca#) than for equivalent phases in octahedral diamonds from Panda and worldwide. Geothermometry of the silicate inclusions yields low equilibration temperatures of 930 to 1010^{o}C. The co-existing fluid micro-inclusions are dominated by H_2O, carbonate and KCl. Fluid inclusions in both the peridotitic and eclogitic samples fall along linear arrays between Fe-Ca-Mg carbonate and KCl. Inclusions in the eclogitic sample also contain moderate concentrations of a Si-Al fluid component, and the eclogitic sample has quartz in its infrared spectra. We suggest that the diamonds have trapped both metasomatised minerals and the metasomatic fluid, and so provide a snap shot of a metasomatic event in the mantle.

Key words: Coated diamond, silicate inclusions, fluid inclusions, metasomatism.

1. Introduction

Fibrous diamonds and the fibrous coats of coated diamonds often contain fluid inclusions trapped along the lateral surfaces of the diamond fibres. The fibrous morphology and presence of fluid inclusions is consistent with rapid diamond growth from a fluid. A remainder of this fluid phase is represented by the inclusions, and provides information on the compositions of the diamond growth fluids [1-7]. These diamonds provide the deepest, and the only pristine, examples of upper mantle fluids. However, to date, it has not been possible to see the whole fluid-rock system. Here we report and examine the relationship between the compositions of co-existing fluid micro-inclusions and peridotitic and eclogitic suite mineral inclusions in the fibrous coats of diamonds from the Panda kimberlite (Canada).

The conditions of diamond growth, such as temperature, pressure and host rock chemistry, are generally determined from the chemistries of non-touching silicate inclusions in diamonds, which are unable re-equilibrate to subsequent changes in the prevailing chemical and physical conditions. 'Macro' inclusion (sizes of the order of 100 μm) minerals of the peridotitic (olivine, Cr-pyrope, orthopyroxene, diopsidic clinopyroxene, chromite), eclogitic (pyrope-almandine garnet and omphacitic clinopyroxene, coesite, kyanite, rutile, sanidine) and "superdeep" (Majoritic garnet,

ferropericlase, stishovite, CaSi and MgSi perovskite) suites constrain the composition of the host mantle. Geothermobarometry of these inclusions indicate that, in the first two cases, they equilibrated at temperatures of 900-1300^{o}C and at depths of 150-200 km [8, 9] in the lithospheric mantle. The sublithospheric diamonds of the third group come from a depth range from 200 to just below the 660 km upper/lower mantle discontinuity [10].

The much smaller fluid 'micro' inclusions (generally < 0.5 μm [11]) present in fibrous diamonds from Botswana and the Democratic Republic of the Congo (DRC) contain fluids that vary between carbonatitic, enriched in Ca, P and CO_2, and silicate rich in Si, Al, K and H_2O [1, 2]. Additionally these fibrous diamonds contain quartz, apatite, mica and carbonates [1, 11-14]. In contrast, fluid in a fibrous diamond coat from the Diavik mine (Canada) ranged in composition from Na-K-Cl brine to Na-rich carbonate [7]. The brine end-member is similar to KCl brine described in internally cloudy diamonds from Koffiefontein (South Africa) [4]. Additionally, primary mantle minerals (Cr-diopside, chromite and olivine) were identified as micro-inclusions phases in the Canadian coated diamond [7] and peridotitic and eclogitic silicates and carbonates were detected as a component of the micro-inclusions in cloudy diamonds from Koffiefontein [5]. However, single phase mineral inclusions have not previously been described from fibrous diamonds.

2. Geological setting, previous work and samples

Panda is a group I (basaltic) kimberlite that intrudes the Central Slave Craton and has a Rb-Sr isochron eruption age of 52.3 ± 3.8 Ma [15]. The xenocryst population of the Panda kimberlite consists of mantle-derived olivine, garnet, pyroxene (Cr-diopside and enstatite), chromite and ilmenite [16]. The lithosphere below Slave consists of two distinct compositional layers [15, 18]: an ultra-depleted hartzburgite-dominated upper layer that straddles the diamond-graphite boundary at 4.2 GPa, 900^{o}C [15], and a deeper layer dominated by more fertile lherzolite.

Silicate mineral inclusions in octahedral diamonds from Panda are dominantly peridotitic (≈85%) [19] and equilibrated at 1100-1250^{o}C [17]. Westerlund et al., [20] derived an age of 3408 ± 280 Ma for peridotitic octahedral diamonds from this kimberlite by Re-Os dating of sulphide inclusions. Eclogitic diamond inclusions include jadeite-poor clinopyroxene and garnet and have not yet been dated. A distinctive feature of the Panda diamond production is the high proportion of coated diamonds, this probably reflects low degrees of diamond resorption during kimberlite ascent [17].

For this study, eight coated diamonds (fibrous diamond ‘coat’ on an octahedral diamond ‘core’) from Panda (0.17-0.29 ct) were made into doubly polished wafers with [100] orientation. The coats are between 26 and 41 mm wide and are milky grey to black. Cathodoluminescence images of all the samples show that the coats are composed of a single growth zone. Prior to analysis, all the samples were cleaned using HCl, acetone and then distilled water. The sample characteristics are summarised in Table 1.

3. Analytical method

Two techniques were principally used in the present study.

3.1 FT-IR

Infrared absorption spectra were collected using a Vector22 Fourier Transform infrared (Ft-ir) spectrometer equipped with a HeNe laser (633 nm), a KBr beam splitter and a deuterated triglycine sulfate (DTGS) detector. The beam diameter was approximately

0.6 mm. Spectra were recorded in transmission with a resolution of 2 cm^{-1} in the range 4000 to 380 cm^{-1} with one spectrum being the average obtained from 512 scans. Polished diamond plates were mounted on a A524 accessory plate with 5x beam condenser. An Al foil mask was used to ensure that only the fibrous coat was analysed. Lattice-bound nitrogen concentrations are determined using the method of Mendelssohn and Milledge [21] (Table 1).

Nitrogen is present as mildly aggregated IaA in all of the diamond coats, this is consistent with global fibrous diamond populations [22-24]. Nitrogen concentrations range between 403 and 1660 ppm in the coats. Lattice bound nitrogen in the Panda diamond cores is more aggregated than in their coats, having up to 33% IaB centres with some platelet development and nitrogen concentrations of 500 to 1540 ppm.

The concentrations of H_2O and carbonate as CO_2 were calculated from the intensities of the O-H stretching band of water (using ε_{3420}=80 L per mol cm^{-1}, [25]) and of the ν_3 stretching band of calcium carbonate (using ε_{1430}=235 L per mol cm^{-1}, [26]). Taking into account the difference in absorption coefficients of different carbonates and the effect of pressure on water and carbonate absorption, the error on the calculated H_2O and CO_2 concentrations are estimated as ±25 and ±40 ppm, respectively [1]. Since the absolute concentration of volatiles is dependent on inclusion density, we use the ratio $H_2O\# = H_2O/(CO_2+H_2O)$ to describe the volatile composition.

Table 1

3.2 Electron microprobe analyses

Electron Microprobe Analyses (EMPA) of individual macro- and micro-inclusions in the diamond coats were performed using a JEOL Superprobe 733. Analyses were carried out using an accelerating voltage of 15 keV and a beam current of 10 nA, at these conditions the spot diameter was approximately 2 µm. The instrument is equipped with an Energy Dispersive Spectrometer (EDS), a collimator and a SiLi crystal detector with an atmospheric thin window (ATW). The channel width is 0.01 KeV and the resolution (the full width half maximum of Mn) is 138 eV. The count rate was 6 to 7 kcps for a count time of 100 s. Spectra were reduced using the Oxford Instruments Link ISIS SEM-Quant (ZAF) correction relative to a cobalt standard.

3.2.1 Macro-inclusions

Silicate inclusions were exposed during polishing of six of the eight Panda coated diamonds. Both peridotitic (PAN1, PAN3, PAN5, PAN7, PAN8) and eclogitic parageneses (PAN4) are represented. Silicate inclusions in the coated diamonds are small (typically 2 to 20 µm) and abundant. Inclusions at the small end of the size range do not give 100% totals. Table 2 shows the analysed total and the normalised molecular proportions of these inclusions. Multiple analysis (20) of a single clinopyroxene grain in PAN4 revealed good reproducibility, with the following standard deviations (1σ): SiO_2 (0.22), Al_2O_3 (0.09), FeO (0.10), Cr_2O_3 (0.08), MgO (0.08), CaO (0.09), TiO_2 (0.12).

Inclusions in the Panda diamond coats are compared to inclusions in octahedral Panda diamonds analysed by WDS. Only differences in the major element concentrations (Mg, Fe, Ca) are considered, because the lower resolution of the EDS. Quoted errors for Mg# (= Mg/(Mg+Fe)) and Ca# (= Ca/(Ca+Mg+Fe)) of each mineral phase are derived by propagating an error of 3σ for the inclusion with the lowest total before normalisation.

Table 2

3.2.2 Micro-inclusions

Individual inclusions were identified immediately below (<1 μm) the surface of the diamond coats using backscattered electron imaging mode. The inclusions are completely enclosed in the diamond host and are not connected to the diamond surface by cracks. Because of the low mean atomic number of diamond, the electron beam shows a significant degree of penetration into the sample with an activation volume of approximately 4 μm^3 at 15 KeV, this is larger than the average inclusion volume (< 1 μm^3).

The small size and high volatile contents of the inclusions means that analysed totals are significantly lower than 100%, the average oxide plus chlorine concentration is 12 wt% (2 to 45 wt%). The sum of oxides plus chlorine was normalised to 100 wt% in order to remove the effect of variable inclusion size, depth and C-O-H content. Normalising the data to 100% assumes a uniform distribution of carbon and oxides in the analysed volume. In actual fact, the inclusions consist of oxides surrounded by carbon matrix therefore low energy x-rays from light elements will be more strongly attenuated. Navon, cited in [5] calculated that this effect has a small effect on most of the analysed elements, but is ~10% for Na, and higher for lighter elements. The accuracy of the analyses of oxides for single inclusions is approximately 10-20% (relative), on the basis of repeated analysis of olivine and clinopyroxene detected in micro-inclusions

The following elements were analysed in the micro inclusions (brackets show the detection limits at 95% confidence): Si (0.05 %), Ti (0.13 %), Al (0.06 %), Mg (0.07 %), Fe (0.15 %), Ca (0.08 %), P (0.08 %), Na (0.08 %), K (0.09 %) and Cl (0.09 %).. The mean of the individual inclusion compositions measured in a sample was taken to represent the bulk major element composition of that sample. The bulk and a selection of representative individual inclusion analyses for each sample are given in Table 3.

4. Results

Table 1

4.1 Macro-inclusions

Olivine, garnet and pyroxene were identified in the infrared spectra of the diamond coats (Fig.1) and from EMPA (Table 1), phlogopite was not detected. No silicate inclusions were observed in the diamond cores.

Figure 1

4.1.1 Garnet

Two diamond coats contain garnet inclusions (PAN8 and PAN5). The garnets have moderate Cr_2O_3 (7.3 to 8.9 wt%) and high CaO contents (5.1 to 6.7 wt%) and are classified as lherzolitic Cr-pyrope (Fig. 2). The chemistry of these garnet inclusions overlap with the compositions of garnet inclusions in octahedral diamonds from Panda [17, 19] and extend the range to more Ca- and Fe-rich compositions. This is reflected in the high values of Ca# of 13.8 to 18.2 (± 1.5).

Figure 2

The Mg# of the garnets varies between 80.6 and 84.3 with an average of 82.0 (± 1.2). The effect of Ca on the Mg–Fe partitioning between garnet and olivine was eliminated by recalculating all garnets to a Ca-free composition according to the method of [17]. From the data of [28], it can be estimated that the Mg# of garnet decreases by 3.0 per cation Ca ([O]=24) at 1000 to 1100^{o}C and 5 GPa, when coexisting with olivine with an Mg# of 91. The recalculated Mg#'s of the Panda garnets vary between 83.4 and 87.1 (mean = 85); the mean Mg# for Slave Cr-pyrope inclusions in diamond is 87.0 and for worldwide samples 87.9 [17]. Therefore, the garnet Mg# values are low.

Low Mg# values are generally considered to be indicative of a high source fertility (i.e. not significantly affected by depletion through partial melting) and low equilibration temperatures. The garnet inclusions also have high Na_2O concentrations (0.2 to 0.40 wt%), a characteristic shared by garnets in octahedral diamonds from Panda [19]. In all the garnets, the TiO_2 concentrations are below the 0.4 wt% cut-off value used as an indicator of metasomatic activity by silicate melts [29, 30].

4.1.2 Olivine

Three of the coated diamonds contain olivine inclusions (PAN1, PAN7 and PAN8). The olivines have forsterite contents of Mg# = 89.7 to 93.1 (± 0.6); this is within the lower half of the worldwide database for inclusions in diamonds and extends the range recorded in olivine inclusions in octahedral Panda diamonds (91.9-93.2 [17, 19]) to lower Mg numbers. In consequence, there is an overlap between the Mg# values of olivine inclusions in the Panda diamond coats and olivine xenocrysts from Panda (generally 90-93, [15]). NiO concentrations range from 0.3 to 0.5 wt% and are within the range of NiO content of inclusions in octahedral diamond from Panda (0.19 to 0.40 wt%, [19]) and worldwide [17].

4.1.3. Clinopyroxene

Eclogitic (PAN4) and peridotitic (PAN3, PAN1, PAN5 and PAN8) clinopyroxenes are represented in the Panda coated diamond inclusion population. Eclogitic clinopyroxene inclusions are found in sample PAN4 and have molar ratios of Mg# = 70.1 to 72.9 and Ca# = to 44.5 to 45.9 and so are omphacitic. Al_2O_3 and Na_2O concentrations are low (7.1 ± 0.3 wt% and 4.7 ± 0.2 wt%, respectively) relative to eclogitic clinopyroxene inclusions from Snap Lake and from worldwide sources. Cr_2O_3 concentrations are generally within or below the detection limit (0.08 wt%).

Peridotitic clinopyroxenes have molar ratios of Mg# = 92.8 to 95.0 (± 1.8) and Ca# = 43.8 to 46.7 (± 1.5); they have Cr_2O_3 concentrations of 1.2 to 2.9 wt% and so are Cr-diopsides. Peridotitic clinopyroxene inclusions are classified as lherzolitic on the basic of their Al_2O_3 and Cr_2O_3 compositions (Fig. 3). These compositions are less magnesian and more Ca-rich than the world average and overlap both with those of clinopyroxene inclusions in octahedral diamonds and clinopyroxene inclusions in xenoliths (91 to 93) from Panda [15, 19].

Figure 3

The Cr-diopside inclusions have Al_2O_3 contents of 0.8 to 2.5 wt% and Na_2O concentrations of 0.7 to 2.3 wt%. Clinopyroxene inclusions in sample PAN3 are compositionally heterogeneous, showing a range of CaO, Al_2O_3, FeO, MgO and Na_2O contents. K_2O concentrations in clinopyroxene inclusions are generally below the

detection limit, and coexist with KCl-bearing fluid micro-inclusions in the Panda diamond coats.

4.1.4 Orthopyroxene

Four orthopyroxene inclusions were analysed, all from PAN3. Like the Cr-pyrope and olivine inclusions, orthopyroxenes have relatively low Mg# values of 89.8 to 92.2 (±1.4).

4.1.5 Inclusion geothermobarometry

We have estimated the temperature of fibrous diamond growth using the non-touching inclusions assemblages in peridotitic samples PAN8 (garnet-olivine, [28, 31]), PAN5 (garnet-clinopyroxene, [32]), PAN1 and PAN5 (enstatite-in-clinopyroxene, [33]). Pressure was estimated using the Cr-in-clinopyroxene barometer of [33] in samples PAN3 and PAN5. The results are given in figure 4 and summarised in table 1.

Figure 4

Geothermobarometry indicates that the peridotitic diamond coats grew at an average temperature of 930-1010 ±50^{o}C and pressures of 4.2 to 4.6 GPa. These conditions are right on the diamond stability line, and overlap with pressure-temperature estimates from xenocrysts in the Panda kimberlite. This may account for the low degree of nitrogen aggregation. These temperatures are slightly lower than those calculated for non-touching pairs of inclusions in non-fibrous diamonds from Panda (1061 to 1233^{o}C, [19]). The calculated PT conditions place the Panda coats on a geotherm of 37 to 40 mW/m^{2} [34], this is slightly lower than for world-wide diamond sources, where geothermal gradients of about 40-42 mW/m^{2} have been deduced [35-37]. The geothermal gradient of the diamond coats are similar to the geothermal gradient indicated by touching garnet and orthopyroxene pairs in Panda octahedral diamonds [17, 19], which have re-equilibrated to the lower mantle temperatures after entrapment in the diamond. The calculated equilibration temperatures are below the lherzolite-H_2O-CO_2 solidus of Wyllie [38].

Compositional disequilibrium in PAN8 leads to wide variations in temperature: calculated temperatures ranging from 730 to 1090^{o}C depending whether low-Mg or high-Mg garnet-olivine pairs were used. The maximum temperature variation calculated within the other samples is <100^{o}C. This wide range calculated temperature in PAN8 is unlikely to be the true temperature range because it is not recorded in the other samples, more likely this reflects varying degrees of disequilibrium between coexisting minerals.

Table 3

4.2 Micro-inclusions

Carbonate and water are present in the infrared spectra of all the Panda diamond coats (Fig. 1). The inclusion spectra are dominated by an intense O-H stretching band in the 2800-3800 cm^{-1} region, due to the presence of hydrogen-bonded O-containing species in the inclusions. The species are identified as molecular H_2O by the strong H_2O ν_2 bending vibration at 1656 cm^{-1} (Fig. 1). The ratio H_2O# ($100H_2O$/ (CO_2+H_2O)) is ≈61 (58 to 70). The broad band centred at 1447 cm^{-1} in both the peridotitic and eclogitic samples is due to the asymmetric stretching vibration (ν_3) of CO_3^{2-} groups [39], whilst the eclogitic sample (PAN4) has a second carbonate peak centred at 1423 cm^{-1} suggesting the presence of a second carbonate species. Quartz is only observed in the single eclogitic

sample. No apatite was detected in the infrared spectra of any of the Panda diamond coats.

In addition to their occurrence as macro-inclusions, olivine (PAN1, PAN2, PAN3, PAN6) and clinopyroxene (PAN1, PAN4, PAN5) are present in the micro-inclusions, where they coexist with K-Na-Cl fluid and/or carbonate. The compositions of these mineral phases are poorly constrained as they are present in very small, multi-phase inclusions. Peridotitic and eclogitic inclusions do not occur mutually within samples. Micro-inclusions containing these mantle silicates are ignored in order to reveal the composition of the coexisting brine and carbonate in the peridotitic and eclogitic samples.

Representative and average major element fluid compositions for each sample are given in table 3. The samples contain Fe-Ca-Mg carbonates, K-Na-Cl brine and silicate; no sulphide was detected. The inclusions span a wide compositional range and the samples are not zoned in terms of major elements.

4.2.1. Peridotitic

Micro-inclusion compositions in the peridotitic coated diamonds from Panda contrast with inclusions in African [1, 2] samples which have higher concentrations of SiO_2 and Al_2O_3. The inclusions are similar to inclusion compositions described in a single fibrous diamond from Diavik [7] (Fig. 5). Fe, Mg and Ca are present in all Panda inclusions and often in the absence of Si and Al. This observation, combined with the presence of carbonate bands in the Ft-ir spectra of all samples, indicates that the micro-inclusions contain carbonate. The average Mg# is 0.42 ±0.1. The peridotitic diamond coat fluids also have high concentrations of Ba (5 - 8 mol%).

The chemistry of the micro-inclusions in the peridotitic diamonds shows that Cl is negatively correlated with Ca, Mg, Fe and Si and positively correlated with K and Na. The average K/Cl molar ratio of the fluid is 0.4 (range 0.07 to 0.71) and the (K+Na)/Cl ratio is 0.6 (range 0.22 to 1.88). The inclusion compositions fall along linear arrays from carbonate towards K-Na-Cl rich compositions (Fig. 5), indicating the presence of a Cl-brine end-member. The calculated end-member carbonate and brine compositions are given in table 3. The brine is similar to the composition of K-Cl rich fluid in cloudy diamonds from Koffiefontein [5] and to the brine end-member fluid in a fibrous diamond from Diavik, Canada [7].

In most inclusions, the molar ratio Na+K/Cl is less than 1, therefore Cl in the inclusions is not fully charge balanced by the alkali cations. However, the sum of the charge associated with positive mono- and divalent (K, Na, Fe, Mg, Ca) ions is >100 (average 223) per 100Cl ions and it is thought that the charge is balanced by carbonate ions as suggested by [4].

Figure 5

4.2.2 Eclogitic

Relative to the peridotitic fluid, the eclogitic fluid is Si- and Al-rich (Fig. 5). The high Si-content is consistent with the presence of quartz, which is observed in the infrared spectra. This chemical composition is similar to published data for fibrous diamonds from Zaire and Botswana [1, 2], but the Panda fluid has a higher concentration of K, Cl and Ba. The eclogitic coat fluid is more Fe-rich (Mg# = 0.2 ±0.1) than that in the peridotitic samples.

In the single eclogitic diamond fluid, Cl is negatively correlated with Ca, Mg, Fe and Si, and correlated with K. In consequence, the inclusion compositions fall along linear arrays from carbonate towards K-Cl rich compositions (Fig. 5), again indicating the presence of a Cl-brine end-member. The average K/Cl molar ratio of the fluid is 0.45 (range 0.07 to 0.60). The calculated composition of the low-Cl and brine end-members is given in table 3. The end-member brine composition in the eclogitic suite micro-inclusions is similar to that in the peridotitic diamond micro-inclusions except for its slightly higher Fe content.

5. Discussion

5.1 Mantle conditions during fibrous diamond growth

The compositions of the silicate inclusions in the Panda diamond coats indicate that fibrous diamonds can grow in both peridotitic and eclogitic host rocks. Therefore, fibrous diamonds grow in the same paragenetic environments as octahedral diamonds. The relatively low Mg# of garnet and olivine in the diamond coats are indicative of high source fertility. Harzburgitic inclusions were not found in the Panda coats, this is in contrast to inclusions in octahedral diamonds from Panda, which are dominantly harzburgitic. Furthermore, the calculated PT conditions of the Panda coats place them within the ultra-depleted upper layer of the Slave lithosphere defined by [15, 18]. The absence of harzburgitic inclusions may be a sampling artefact due to the fact that there are only eight Panda coated diamonds in this study. Alternatively, the dominance of lherzolitic inclusions may suggest that the diamond coats formed during a localized refertilization event involving the influx of the coexisiting Ca-rich fluid, which converted harzburgite to lherzolite.

Geothermometry of silicate macro-inclusions indicates that the Panda diamonds grew over a narrow temperature range of 930 to 1010^{o}C. These calculated temperatures from EDS analyses are lower than indicated by inclusions in non-fibrous diamonds from Panda (1100-1250^{o}C, [19]). For the amount of nitrogen present, the low degree of nitrogen aggregation is also consistent with temperatures <1200^{o}C. Diamond growth at lower temperatures may be possible because of the high level of fluid supersaturation, which is consistent with the development of a fibrous morphology. Synthetic diamonds grown in KCl [40] and carbonate-KCl [41] exhibit skeletal forms, testifying to high crystallisation rates in KCl-bearing systems. Geobarometry gives calculated equilibration pressures of 4.2-4.6 GPa for Panda coat inclusions.

The pressure-temperature conditions indicated by inclusion geothermobarometry of the lherzolitic Panda diamond coats fall just below the lherzolite + H_2O + CO_2 solidus of Wyllie et al., [42]. This is consistent with the presence of liquid water in all samples and the absence of silicate melt in the peridotitic Panda diamond coats. These low temperatures also suggest that fibrous diamonds growth at Panda was not the result of a thermal event and favours a growth model driven by open system arrival of externally derived metasomatic fluids.

5.2 Origin of the silicate inclusions

The silicate inclusions in the Panda diamond coats are smaller and more abundant than silicate inclusions in octahedral diamonds. The macro-inclusions in the diamond coats may either be 1) syngenetic inclusions precipitated directly from a melt; precipitation of silicate and diamond left a residual carbonate-KCl-H_2O fluid; or 2) protogenetic inclusions from the mantle host which coexisted with the fluid from which diamond

precipitated. Survival of the diamond cores is an important criterion for both of these models. These events are not thought to be late stages of core growth (i.e. from the residual melt) because the sharp boundary, and the difference in nitrogen aggregation states between the core and coat suggests that the two formed at separate times.

In the syngenetic scenario, the presence of both eclogitic and peridotitic silicate inclusions in the diamond coats indicates that fibrous diamond growth occurred during at least two events involving silicate-bearing melts. The small size and abundance of the silicate inclusions may reflect conditions in the growth environment: small and abundant minerals suggest that the nucleation rate was higher than the growth rate during crystallisation. High levels of nucleation are generally attributed to supersaturation of the growth medium and/or to undercooling (growth temperature lower than saturation temperature). Silicate supersaturation of the fibrous diamond coat growth environment is considered unlikely because of the low Si-content of the trapped fluid. The H_2O-rich nature of the coexisting fluid suggests that diffusion was unlikely to be slow, so the growth rate should not have limited the size of silicate crystals. The low equilibration temperatures are not inconsistent with undercooling, however rapid cooling is not considered likely in the upper mantle.

In the protogenetic scenario, the silicate macro-inclusions represent the host rock in which the diamond cores resided, and which has been modified by an incoming carbonate-H_2O metasomatic fluid similar to that trapped in the micro-inclusions. Significant melting/crystallisation of the silicate host rock did not occur in this scenario, this is consistent with the equilibration temperatures of the silicate inclusions, which are below the lherzolite+H_2O+CO_2 solidus. In this scenario, the small size of the silicate inclusions is due to preferential uptake of smaller crystals. This model is more consistent with the carbonate-rich, Si-poor nature of the trapped fluid.

5.3 Nature of the trapped fluid

All the of the Panda diamond coat micro-inclusions contain H_2O and have carbonate and KCl in varying proportions. The similarity between the compositions of carbonate in the peridotitic and eclogitic samples suggests that this fluid may have been derived externally and percolated through both paragenetic environments. In this scenario, the peridotitic and eclogitic diamond coats grew in the same metasomatic event.

Klein-BenDavid et al., [7] suggest that the carbonatite melt evolves towards a more KCl-rich composition by mineral crystallisation. During late stage crystallisation, the residual melt/fluid will contain a higher concentration of KCl and Ba. This mechanism may explain the small scale variations in observed micro-inclusion compositions. Olivine and clinopyroxene found in the some of the fluid micro-inclusions may be precipitates from such a carbonatite melt. The very high K and Cl concentrations of the Panda fluids suggest that the brine was not sourced locally, but from a large volume of the mantle. Burgess et al., [43] measured halogen ratios in coated diamonds from Panda and concluded that high I/Cl and Br/Cl ratios also require the fluids to have acquired halogens from a large volume of the mantle.

The carbonate-, KCl- and H_2O-rich fluid inclusions represent the residual fluid after precipitation of diamond. The prevailing oxidation state during fluid influx and diamond coat formation is constrained by the need for diamond to remain stable throughout, so that the diamond cores are preserved. The upper limit of diamond stability in lherzolite is defined by the reaction: enstatite + magnesite = forsterite + diopside + diamond

(EMFDD), which occurs approximately -1.5 log fO_2 below the fayalite-magnetite-quartz buffer [44]. Diamond and carbonate may co-exist at this reaction line. The diamond coat may have formed from the parental C-bearing fluid, either by reduction of an oxidized fluid, such as carbonate or CO_2, or by the oxidation of a reduced fluid, such as CH_4: 1) If the initial fluid was reducing, then oxidation would drive the fluid composition to higher fO_2. The fluid would initially precipitate diamond and carbonate would only form once the EMFDD buffer was intersected. However, CH_4 is not detected in the Ft-ir spectra of the diamond coats and carbonate is not concentrated towards the rim of the diamond coats. Furthermore, in this scenario, carbonate is formed at the expense of diamond. 2) If the initial fluid was oxidising, then the fO_2 of the fluid must have been lowered by reaction with the more reducing host mantle. Once the fluid intersected the EMFDD buffer, diamond would have been precipitated at the expense of carbonate. The reduction process was buffered by the formation of diamond, this allowed carbonate to coexist with diamond throughout the growth of the coat. This is consistent with the lack of zoning in the diamond coats. The redox state if the host mantle is raised slightly during interaction with the incoming fluid, but do not increase above the EMFDD buffer, therefore the diamond cores remain stable throughout. The similarity between the composition of the carbonate components in the peridotitic and eclogitic samples also support the suggestion that the incoming fluid was carbonate-rich, rather than reducing. Therefore, we suggest that this fluid was then reduced by interaction with the minerals of the host rock to form the fibrous diamond coats.

The Si-rich fluid component, which is virtually absent in the peridotitic samples, is an important component of the fluid in the single eclogite sample. This is emphasized by the presence of quartz in the inclusions. This suggests that this silicate end-member fluid component may have been derived locally. In the eclogitic Panda fluid, the minor silicate component may be due to either: 1) partial melting of the eclogite host rock as a result of the lower temperature of the eclogite + H_2O solidus; or 2) to the greater availability of Al and Si in minerals in the solid eclogite host rock, which may be liberated by metasomatic reactions between fluid and host rock minerals. In both these scenarios, the silicate fluid component is generated locally. SiO_2 is thought to have crystallized from the trapped silicate fluid component.

Figure 6

5.4 Relationship between the diamond core and its coat

For the purposes of this section, we assume that the Panda diamond cores are part of the same diamond population as normal octahedral diamonds sampled by the Panda kimberlite. The similarity between the nitrogen content and degree of nitrogen aggregation in the diamond cores in this study and of undeformed octahedral diamonds from Panda [1, 45] suggests that the populations may be broadly contemporaneous.

The contrasting nitrogen characteristic of the diamond core and its coat suggests that they grew during separate events. This is supported by the sharp boundary between the core and coat in the CL image. Nitrogen in the cores is more aggregated (up to ~30% IaB centres) than in the coat (100% IaA), suggesting that the growth of the coat was succeeded by a period of mantle residence prior to the growth of the coat. Growth during separate events is supported by the lower equilibration temperature of the coat inclusions, relative to those in Panda octahedral diamonds [19]. Therefore we assume that the growth of the diamond cores, which are equivalent to normal octahedral diamonds, occurred some time before the growth of their fibrous coats, and that the host

mantle cooled by approximately 200°C in the intervening period. If the macro inclusions are indeed protogenetic, then the diamond coat inclusions come from the same host rocks as those in octahedral diamonds from Panda [17, 19], so may be directly compared.

The coat inclusions extend the compositional range of Panda diamond inclusion compositions from relatively undepleted inclusions in octahedral diamonds [17, 19] to more fertile Fe- and Ca-rich compositions (lower Mg# and higher Ca#). When compared to the composition of the trapped fluid (Fig. 6), it can be seen that the compositions of garnet, olivine and orthopyroxene inclusions in the Panda diamond coats are more Fe-rich, and garnet and orthopyroxene are more Ca-rich than equivalent minerals in octahedral Panda diamonds. The trend between the compositions of octahedral and coat inclusion compositions is towards the composition of the Fe- and Ca-rich carbonate observed in the coat micro-inclusions. This suggests that the inclusions in the diamond coats may be protogenetic and, if so, the differences between octahedral diamond and diamond coat inclusion compositions provide a snap-shot of mantle metasomatism. This metasomatic event was probably localised, for example to vein walls, firstly because H_2O-rich fluids have high dihedral angles in mantle rocks: ~40° in dunite [46] and higher in multi-mineralic peridotites; and >60° in eclogite [47] at 5 GPa. The diamond-forming H_2O-CO_2 fluids can thus only infiltrate grain edges under conditions of high fluid volume or host-rock deformation. Secondly, because most xenoliths from < 5 GPa are ultra-depleted harzburgite [15, 18].

6. Conclusions

Panda diamond coats contain macro-inclusions of olivine, garnet, orthopyroxene and clinopyroxene. Both peridotitic (lherzolitic) and eclogitic suite minerals are represented, therefore fibrous diamonds may grow in the same paragenetic environments as octahedral diamonds. The calculated equilibration temperatures for the peridotitic coat inclusions (930 to 1010°C) are lower than indicated by inclusions in octahedral diamonds from Panda (1100-1250°C;[19]) and fall below the lherzolite+H_2O+CO_2 solidus [38]. The silicate inclusions have low values of Mg# and have higher Ca# values than equivalent minerals in octahedral diamonds from Panda [17, 19]. The coat inclusion compositions trend away from those of equivalent phases in octahedral diamonds from Panda in the direction of the trapped fluid. This suggests that, if the silicate inclusions in the coat are protogenetic, then chemical difference between inclusions in octahedral diamonds and those in the diamond coats record the effect of mantle metasomatism.

The co-existing fluid micro-inclusions are dominated by H_2O, carbonate and KCl. Fluid inclusions in both the peridotitic and eclogitic samples fall along linear arrays between Fe-Ca-Mg carbonate and KCl. Inclusions in the peridotitic samples contain very low or zero concentrations of Si-Al and do not contain quartz. In contrast, inclusions in the eclogitic sample do contain moderate concentrations of a Si-Al fluid component, and the eclogitic sample has quartz in its infrared spectra. Therefore, the eclogitic Panda sample bears some resemblance to fluids in coated diamonds from Africa [1, 2], but has a higher KCl content. We suggest that the carbonate-H_2O-KCl fluid component may have been externally derived and percolated through both peridotitic and eclogitic diamond (core) bearing mantle. Metasomatism of the host mantle modified the fluid composition, leading to a higher Si-Al content in eclogite. Diamond precipitated from this fluid, and the micro-inclusions represent the residue after metasomatism and mineral (including diamond) precipitation.

Acknowledgements: This work is funded by and EPSRC (award no. 01302499) industrial CASE studentship with DeBeers. Andy Taylor and Jacques Jones (DTC research, Maidenhead) are thanked for laser cutting and sample preparation. Prof Thomas Stachel, Dr Ray Burgess, Dr Andy Beard and an anonymous reviewer are thanked for valuable feedback in review.

References

[1] O. Navon, I.D. Hutcheon, G.R. Rossman and G.J. Wasserburg, Mantle-derived fluids in diamond micro-inclusions, Nature 335, 784-789, 1988.

[2] M. Schrauder and O. Navon, Hydrous and Carbonatitic Mantle Fluids in Fibrous Diamonds from Jwaneng, Botswana, Geochimica Et Cosmochimica Acta 58(2), 761-771, 1994.

[3] M. Schrauder, C. Koeberl and O. Navon, Trace element analyses of fluid-bearing diamonds from Jwaneng, Botswana, Geochimica Et Cosmochimica Acta 60(23), 4711-4724, 1996.

[4] E.S. Izraeli, J.W. Harris and O. Navon, Brine inclusions in diamonds: a new upper mantle fluid, Earth and Planetary Science Letters 187(3-4), 323-332, 2001.

[5] E.S. Izraeli, J.W. Harris and O. Navon, Fluid and mineral inclusions in cloudy diamonds from Koffiefontein, South Africa, Geochimica Et Cosmochimica Acta 68(11), 2561-2575, 2004.

[6] O. Klein-BenDavid, E.S. Izraeli and O. Navon, Volatile-rich brine and melt in Canadian diamonds, Geochimica Et Cosmochimica Acta 66(15A), A403-A403, 2002.

[7] O. Klein-BenDavid, E.S. Izraeli, E. Hauri and O. Navon, Mantle fluid evolution—a tale of one diamond, Lithos 77, 243-253, 2004.

[8] H.O.A. Meyer, Inclusions in diamond, Mantle Xenoliths, Published by Wiley-Interscience, Editors Nixon P.H., 501-522, 1987.

[9] J.W. Harris, Diamond geology., in: The Properties of Natural and Synthetic Diamonds, J.E. Field, ed., pp. 384–385, Academic Press,, Oxford, UK, 1992.

[10] T. Stachel, Diamonds from the asthenosphere and the transition zone, European Journal of Mineralogy 13(5), 883-892, 2001.

[11] G.D. Guthrie, D.R. Veblen, O. Navon and G.R. Rossman, Sub-micrometer Fluid Inclusions in Turbid-Diamond Coats, Earth and Planetary Science Letters 105(1-3), 1-12, 1991.

[12] A.R. Lang and J.C. Walmsley, Apatite Inclusions in Natural Diamond Coat, Physics and Chemistry of Minerals 9(1), 6-8, 1983.

[13] J.C. Walmsley and A.R. Lang, On Sub-micrometer Inclusions in Diamond Coat - Crystallography and Composition of Ankerites and Related Rhombohedral Carbonates, Mineralogical Magazine 56(385), 533-543, 1992.

[14] J.C. Walmsley and A.R. Lang, Oriented Biotite Inclusions in Diamond Coat, Mineralogical Magazine 56(382), 108-111, 1992.

[15] A. Menzies, K. Westerlund, H. Grutter, J. Gurney, J. Carlson, A. Fung and T. Nowicki, Peridotitic mantle xenoliths from kimberlites on the Ekati Diamond Mine property, NWT, Canada: major element compositions and implications for the lithosphere beneath the central Slave craton, Lithos 77(1-4), 395-412, 2004.

[16] T. Nowicki, B. Crawford, D. Dyck, J. Carlson, R. McElroy, P. Oshust and H. Helmstaedt, The geology of kimberlite pipes of the Ekati property, Northwest Territories, Canada, Lithos 76(1-4), 1-27, 2004.

[17] T. Stachel, J.W. Harris, R. Tappert and G.P. Brey, Peridotitic diamonds from the Slave and the Kaapvaal cratons - similarities and differences based on a preliminary data set, Lithos 71(2-4), 489-503, 2003.

[18] W.L. Griffin, B.J. Doyle, C.G. Ryan, N.J. Pearson, S.Y. O'Reilly, R. Davies, K. Kivi, E. Van Achterbergh and L.M. Natapov, Layered mantle lithosphere in the Lac de Gras area, Slave Craton: Composition, structure and origin, Journal of Petrology 40(5), 705-727, 1999.

[19] R. Tappert, T. Stachel, J.W. Harris, N. Shimizu and G.P. Brey, Mineral inclusions in diamonds from the Panda kimberlite, Slave Province, Canada, European Journal of Mineralogy 17(3), 423-440, 2005.
[20] K.J. Westerlund, S.H. Shirley, S.H. Richardson, J.J. Gurney and J.W. Harris, Re-Os systematics of diamond inclusion sulfides from the Panda kimberlite, Slave craton, in: Extended Abstracts of the 8th International Kimberlite Conference, pp. FLA_0134, Victoria, Canada, 2003.
[21] M.J. Mendelssohn and H.J. Milledge, Geologically significant information from routine analysis of the mid-infrared spectra of diamonds, International Geology Review 37, 95-110, 1995.
[22] S.R. Boyd, D.P. Mattey, C.T. Pillinger, H.J. Milledge, M.J. Mendelssohn and M. Seal, Multiple growth events during diamond genesis: an integrated study of carbon and nitrogen isotopes and nitrogen aggregation state in coated stones, Earth and Planetary Science Letters 86, 341-353, 1987.
[23] S.R. Boyd, C.T. Pillinger, H.J. Milledge and M.J. Seal, C-Isotopic and N-Isotopic Composition and the Infrared- Absorption Spectra of Coated Diamonds - Evidence for the Regional Uniformity of CO_2-H_2O Rich Fluids in Lithospheric Mantle, Earth and Planetary Science Letters 108(1-3), 139-150, 1992.
[24] S.R. Boyd, F. Pineau and M. Javoy, Modeling the Growth of Natural Diamonds, Chemical Geology 116(1-2), 29-42, 1994.
[25] W.K. Thompson, Infra-red spectroscopic studies of aqueous systems. Part 1.—Molar extinction coefficients of water, deuterium oxide, deuterium hydrogen oxide, aqueous sodium chloride and carbon disulphide, Transactions of the Faraday Society 61, 2635-2640, 1965.
[26] G. Fine and E. Stolper, The Speciation of Carbon-Dioxide in Sodium Aluminosilicate Glasses, Contributions to Mineralogy and Petrology 91(2), 105-121, 1985.
[27] L.H. Johnson, R. Burgess, G. Turner and J.W. Harris, Noble gas and halogen geochemistry of mantle fluids: Comparison of African and Canadian diamonds, Geochimica Et Cosmochimica Acta 64(4), 717-732, 2000.
[28] H.S. O'Neill, An experimental study of FeMg partitioning between garnet and olivine and its calibration as a geothermometer, Contributions to Mineralogy and Petrology 70, 59-70, 1978.
[29] J.J. Gurney, B. Harte and K.G. Cox, Mantle xenoliths in the Matsoku kimberlite pipe., Physics and Chemistry of the Earth 9, 507-529, 1975.
[30] M. Matthews, B. Harte and D. Prior, Mantle Garnets - a Cracking Yarn, Geochimica Et Cosmochimica Acta 56(7), 2633-2642, 1992.
[31] H.S. O'Neill, An experimental study of FeMg partitioning between garnet and olivine and its calibration as a geothermometer: corrections, Contributions to Mineralogy and Petrology 72, 337, 1980.
[32] E.J. Krogh, The Garnet-Clinopyroxene Fe-Mg Geothermometer - a Reinterpretation of Existing Experimental-Data, Contributions to Mineralogy and Petrology 99(1), 44-48, 1988.
[33] P. Nimis and W.R. Taylor, Single clinopyroxene thermobarometry for garnet peridotites. Part I. Calibration and testing of a Cr-in-Cpx barometer and an enstatite-in-Cpx thermometer, Contributions to Mineralogy and Petrology 139(5), 541-554, 2000.
[34] H.N. Pollack and D.S. Chapman, On the regional variation of heat flow, geotherms, and lithospheric thickness, Tectonophysics 38, 279-296, 1977.
[35] F.R. Boyd and J.J. Gurney, Diamonds and the African lithosphere, Science 232, 472-477, 1986.

[36] W.L. Griffin, J.J. Gurney and C.G. Ryan, Variations in trapping temperatures and trace elements in peridotite-suite inclusions from African diamonds - Evidence for two inclusion suites, and implications for lithosphere stratigraphy, Contributions to Mineralogy and Petrology 110, 1-15, 1992.
[37] T. Stachel and J.W. Harris, Syngenetic inclusions in diamond from the Birim field (Ghana) - A deep peridotitic profile with a history of depletion and re- enrichment, Contributions to Mineralogy and Petrology 127(4), 336-352, 1997.
[38] P.J. Wyllie, Experimental Petrology of Upper-Mantle Materials, Process and Products, Journal of Geodynamics 20(4), 429-468, 1995.
[39] White, The carbonate minerals, in: The infrared spectra of minerals, V.C. Farmer, ed., pp. 227-284, Mineralogical Society, London, 1974.
[40] Y.A. Litvin, Alkaline-chloride components in processes of diamond growth in the mantle and high-pressure experimental conditions, Doklady Earth Sciences 389(3), 388-391, 2003.
[41] E. Tomlinson, A. Jones and J. Milledge, High-pressure experimental growth of diamond using C-K_2CO_3-KCl as an analogue for Cl-bearing carbonate fluid, Lithos 77(1-4), 287-294, 2004.
[42] P.J. Wyllie and I.D. Ryabchikov, Volatile components, magmas, and critical fluids in upwelling mantle, Journal of Petrology 41(7), 1195-1206, 2000.
[43] R. Burgess, D. Harrison, E. Hobson, P. Cartigny and J. Harris, Volatile Composition of Canadian Fibrous Diamonds: Implications for the Origin and Fractionation of Halogens in the mantle, in: in prep, 2005.
[44] R.W. Luth, Diamonds, Eclogites, and the Oxidation-State of the Earths Mantle, Science 261(5117), 66-68, 1993.
[45] K.J. Westerlund, J.J. Gurney, S.B. Shirey and E. Hauri, Nitrogen Aggregation and Stable Nitrogen and Carbon Isotope Characteristics of Diamonds from the Panda Kimberlite, Slave Craton, Canada, in: Slave-Kaapvaal Workshop: A Tale of Two-Cratons, Merrickville, Ontario, 2001.
[46] K. Mibe, T. Fujii and A. Yasuda, Connectivity of aqueous fluid in the Earth's upper mantle, 25(8), 1233-1236, 1998.
[47] K. Mibe, T. Yoshino, S. Ono, A. Yasuda and T. Fujii, Connectivity of aqueous fluid in eclogite and its implications for fluid migration in the Earth's interior, Journal of Geophysical Research-Solid Earth 108(B6), art. no.-2295, 2003.
[48] R. Berman and R. Simon, On the Graphite-Diamond Equilibrium, Zeit. Elektrochem. 59, 333-338, 1955.

Figure captions

Figure 1: Infrared absorption spectra of selected Panda diamond coats. The original spectra shown by the grey line, the black line shows the result after subtraction of the residual IaA diamond spectrum. All spectra show a wide absorption band at ≈3440 cm^{-1} and the band at ≈1652 cm^{-1} is due to the presence of OH. Minerals present include: olivine (PAN1: 887, 507, 987, 608, 532 and 843 cm^{-1}), pyroxene (PAN4: 1090, 480, 877 (shoulder), 520, 977, 908, 644 cm^{-1}), garnet (PAN5: 484, 877, 904 (shoulder), 575, 967, 993 cm^{-1}), quartz (PAN4: 812 and 784 cm^{-1}) and carbonate (880 and 1460-1420 cm^{-1}). Additionally, all samples have a sharp peak at 3107 cm^{-1} due to lattice bound hydrogen.

Figure 2: Cr_2O_3 verses CaO for garnet inclusions in diamond coats PAN5 (large open triangles) and PAN8 (large open squares). Also shown are compositions of garnet inclusions in octahedral diamonds from Panda, data from [17, 19] (small closed circles) and of garnets from Panda peridotite xenoliths from [15] (small diamonds).

Figure 3: Al_2O_3 verses Cr_2O_3 for clinopyroxene inclusions in Panda coated diamonds (large symbols). Also shown are compositions of clinopyroxene inclusions in octahedral diamonds from Panda, data from [17] (closed circles) and mantle xenoliths from Panda (small open diamonds) [15].

Figure 4: Average pressure-temperature conditions of clinopyroxene equilibration in samples PAN3 and PAN5 calculated using [33] (error bars show the range of conditions calculated using the full range of compositions), and the temperature of PAN8 calculated for a range of pressures (dark grey line) calculated using the garnet-olivine geothermometer of [28, 31]. Black circles are the temperatures of formation of non-touching pairs of garnet-olivine inclusions in octahedral diamonds from Panda calculated at 5 GPa; the light shaded area represents the range of temperatures at given pressures of inclusions in octahedral diamonds [19] and of clinopyroxene crystals in mantle xenoliths (solid black circles) from Panda (open diamonds) [15] calculated using [33]. Dashed lines show conductive geotherms (in mW/m^2) for various surface heat flow values are calculated after [34], the graphite-diamond stability boundary is shown as a solid black line [48].

Figure 5: Compositions of micro-inclusions in peridotitic (grey diamonds; PAN1, PAN2, PAN3, PAN5, PAN6, PAN7, PAN8) and eclogitic (black diamonds; PAN4) coated diamonds from Panda. Also shown are published data from coated diamonds from Africa [1, 2] (open squares) and Diavik (Canada) [7] (open triangles) cloudy diamonds from Koffiefontein [4] (open circles). Summary insets show the compositional fields of inclusions in the peridotitic (P, grey) and eclogite (E, black) samples.

Figure 6: Ternary diagram showing the compositions of garnet (squares), olivine (circles), orthopyroxene (diamonds) and clinopyroxene (triangles) inclusions in octahedral diamonds (grey-filled symbols) [17, 19] and the fibrous diamond coats (open symbols) and of the average fluid composition (cross) and field of measured fluid compositions (grey filled area) in micro-inclusions in the coat. Garnet, opx and olivine in the diamond coat trend away from the composition of equivalent minerals in octahedral diamond in the direction of the trapped fluid composition.

Table 1: Summary of Panda diamond coat characteristics determined from Ft-ir spectroscopy and EMPA. Nitrogen aggregation state quotes as percentage of IaB

aggregate in core. Nitrogen and H_2O concentrations are given in ppm. H_2O=100H_2O/(H_2O+CO_2). Mineral phases as detected in: [x]Ft-ir absorption spectra, EMPA as [y]single phase macro-inclusions [z]micro-inclusion phases. Pressure and temperature conditions are calculated from macro-inclusion compositions using the geothermometers of [a][28, 31], [b][32] and the geothermobarometer of [c][33]. Starting pressures for calculation were 4.6 GPa, indicated as the most appropriate pressure by geobarometry.

Table 2: EMPA analyses of silicate inclusions in diamond coats from Panda. Totals are normalised to 100 wt% and the analysed total is given, the analysed totals are also given. Mg# = Mg/(Mg+Fe), Ca# = Ca/(Ca+Mg+Fe). Abbreviations: lherz. - lherzolite, ecl. - eclogite, nd - not detected.

Table 3: Compositions of fluid inclusions in coated diamonds from Panda. The average and standard deviation are given for each sample, in addition to four (peridotitic) or ten (eclogitic) representative inclusion compositions. The total molecular proportions and the total oxide plus chlorine contents are normalised to 100 wt%, with the analysed total also given. The calculated brine and carbonate end-members for the peridotite and eclogite suite inclusions and also given.

Fig. 1

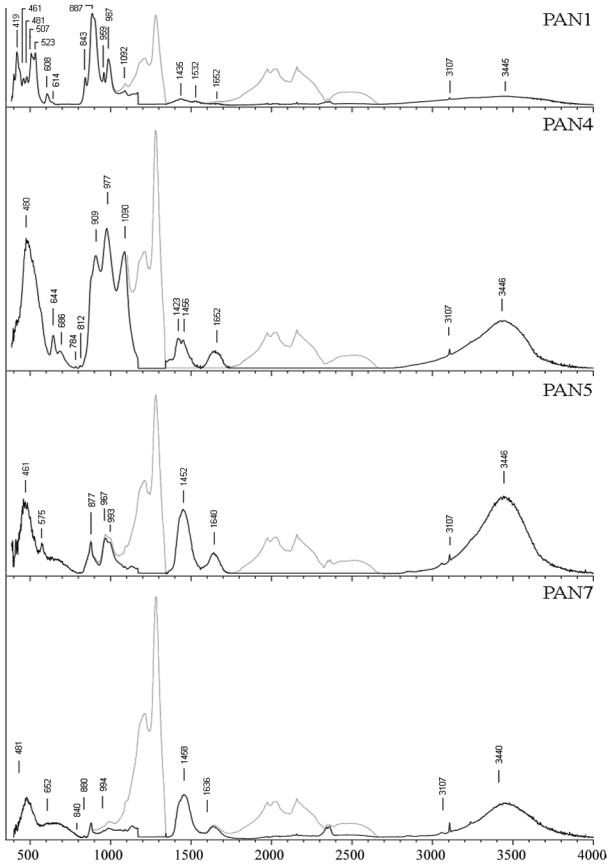

Figure 2

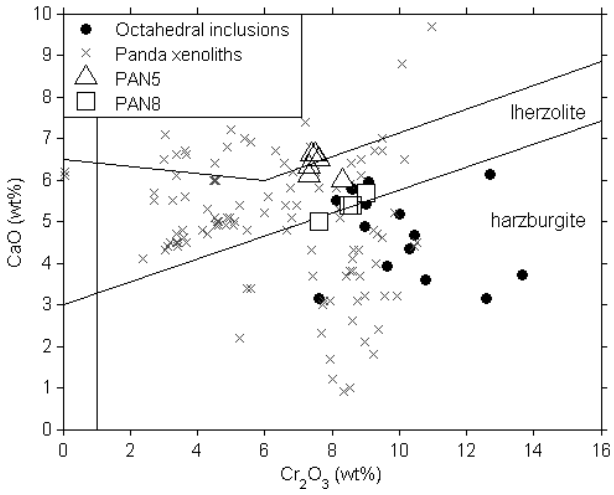

Figure 3:

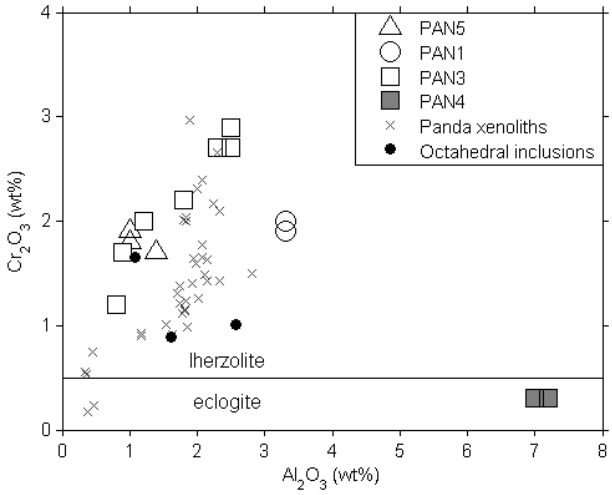

Figure 4:

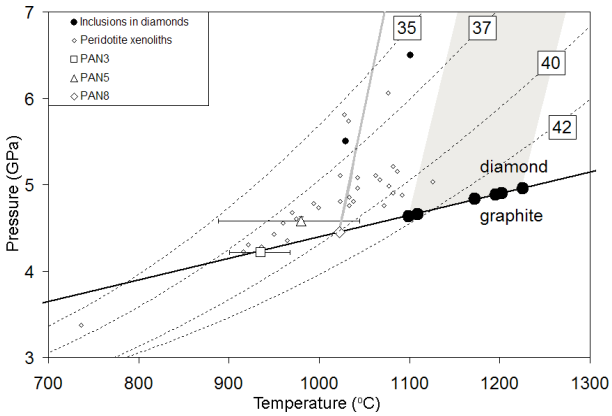

Figure 5:

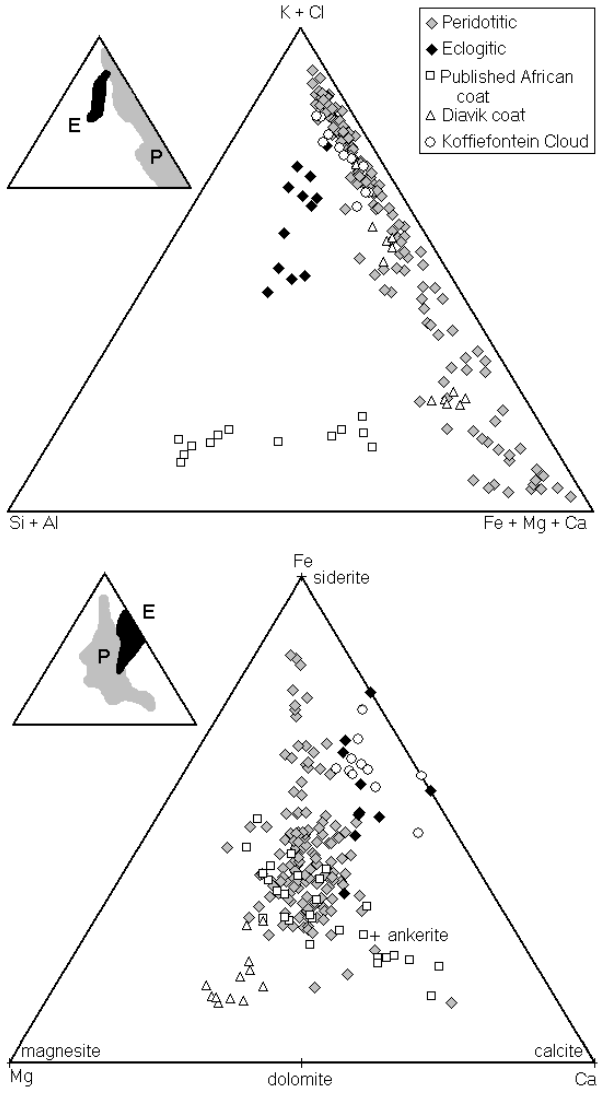

Figure 7:

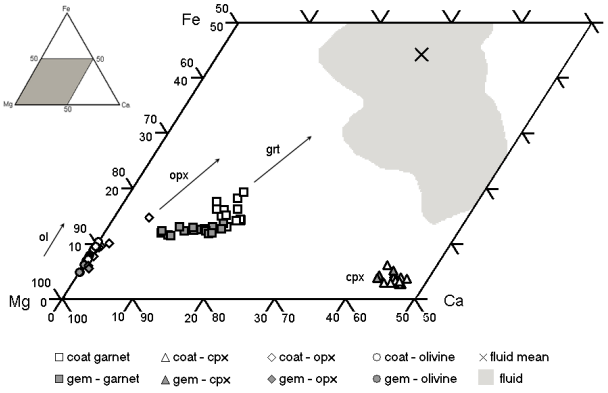

	core		coat						
Sample	N	%B	Suite	N	H_2O	H_2O#	Minerals present	T (^oC)	P (Gpa)
PAN1	-	-	P	580	61	68	olivine^{xyz}, cpx^{yz}, carb.^{x}		
PAN2	500	33	P	405	33	64	olivine^{z}, carb.^{x}		
PAN3	-	-	P	1345	351	63	pyroxene^{x}, (cpx^{y},opx^{y}), carb.^{x}	935[c]	4.2[c]
PAN4	-	-	E	1560	354	68	cpx^{xyz}, rutile^{y}, quartz^{x}, carb.^{x}		
PAN5	585	30	P	1270	564	59	garnet^{xy}, cpx^{yz}, carb.^{x}	959[b], 980[c]	5.4[c]
PAN6	1040	10	P	600	31	56	olivine^{z}, carb.^{x}		
PAN7	1550	8	P	1660	248	55	olivine^{y}, carb.^{x}		
PAN8	1200	3	P	845	251	56	garnet^{y}, olivine^{y}, carb.^{x}	1006[a]	

Suite	Sample	SiO_2	TiO_2	Al_2O_3	Cr_2O_3	FeO	NiO	MgO	CaO	Na_2O	K_2O	total	Si	Ti	Al	Cr	Fe	Mg	Ca	Na	Mg#	Ca#
Garnet																						
lherz.	PAN8	41.4	0.2	16.7	8.5	7.4	0.2	17.9	5.4	0.3	0.7	66.1	6.1	0.02	2.9	1.0	0.9	3.9	0.8	0.1	81.1	14.9
lherz.	PAN8	41.9	nd	17.1	8.6	6.9	nd	18.1	5.4	0.3	0.4	91.2	6.1	-	2.9	1.0	0.8	3.9	0.8	0.1	82.3	15.1
lherz.	PAN8	41.8	0.2	17.5	7.6	7.5	nd	18.2	5.0	0.4	0.8	101.8	6.1	0.02	3.0	0.9	0.9	4.0	0.8	0.1	81.2	13.8
lherz.	PAN8	41.4	0.1	16.9	9.0	7.0	nd	18.0	5.7	0.4	0.1	79.7	6.0	0.01	2.9	1.0	0.9	3.9	0.9	0.1	82.1	15.6
lherz.	PAN5	42.8	0.1	18.0	7.3	6.1	nd	18.5	6.1	0.2	nd	99.8	6.2	0.01	3.1	0.8	0.7	4.0	0.9	0.1	84.3	16.8
lherz.	PAN5	42.5	nd	17.9	7.4	6.6	0.1	17.7	6.6	0.2	nd	101.1	6.2	-	3.1	0.8	0.8	3.8	1.0	0.1	82.7	18.2
lherz.	PAN5	41.2	nd	17.6	8.3	7.4	nd	17.3	6.0	0.3	0.5	59.3	6.0	-	3.0	1.0	0.9	3.8	0.9	0.1	80.6	16.8
lherz.	PAN5	42.1	nd	17.9	7.5	6.6	0.2	17.6	6.6	0.2	0.1	87.6	6.1	-	3.1	0.9	0.8	3.8	1.0	0.1	82.6	18.2
lherz.	PAN5	42.4	nd	17.9	7.6	6.7	nd	17.6	6.5	0.2	nd	99.7	6.2	-	3.1	0.9	0.8	3.8	1.0	0.1	82.4	18.0
lherz.	PAN5	42.8	nd	18.1	7.3	6.5	nd	17.7	6.3	0.2	0.1	101.1	6.2	-	3.1	0.8	0.8	3.8	1.0	0.1	82.9	17.5
Clinopyroxene																						
lherz.	PAN5	54.6	nd	1.0	1.9	2.1	nd	17.3	21.8	1.2	nd	55.2	2.0	-	0.0	0.1	0.1	0.9	0.8	0.1	93.6	45.9
lherz.	PAN5	55.4	nd	1.0	1.9	1.6	nd	17.0	21.7	1.1	nd	68.8	2.0	-	0.0	0.1	0.0	0.9	0.8	0.1	94.9	46.6
lherz.	PAN5	56.9	0.1	1.0	nd	1.7	nd	17.3	22.0	1.0	nd	83.8	2.0	0.00	0.0	-	0.0	0.9	0.8	0.1	94.9	46.4
lherz.	PAN5	56.2	nd	1.0	1.8	1.6	nd	16.9	21.3	1.0	nd	84.9	2.0	-	0.0	0.1	0.0	0.9	0.8	0.1	95.0	46.3
lherz.	PAN5	55.0	nd	1.4	1.7	1.8	nd	17.8	20.6	1.1	0.3	52.1	2.0	-	0.1	0.0	0.1	1.0	0.8	0.1	94.6	44.0
lherz.	PAN1	56.3	0.1	3.3	1.9	2.2	0.2	15.0	18.4	2.3	nd	80.1	2.0	0.00	0.1	0.1	0.1	0.8	0.7	0.2	92.4	44.9
lherz.	PAN1	55.9	0.1	3.3	2.0	2.4	nd	15.2	18.5	2.4	nd	73.6	2.0	0.00	0.1	0.1	0.1	0.8	0.7	0.2	91.8	44.6
lherz.	PAN3	55.0	0.3	1.2	2.0	2.3	nd	16.6	21.2	1.0	0.1	87.7	2.0	0.01	0.0	0.1	0.1	0.9	0.8	0.1	92.8	46.0
lherz.	PAN3	56.0	0.3	2.5	2.9	1.7	nd	15.3	18.9	2.2	nd	85.4	2.0	0.01	0.1	0.1	0.1	0.8	0.7	0.2	94.2	45.5
lherz.	PAN3	56.2	0.2	0.9	1.7	2.2	nd	16.2	21.4	0.9	nd	91.5	2.0	0.01	0.0	0.0	0.1	0.9	0.8	0.1	93.1	46.9
lherz.	PAN3	55.4	0.4	2.5	2.7	2.1	nd	15.7	19.1	1.8	0.3	88.6	2.0	0.01	0.1	0.1	0.1	0.8	0.7	0.1	93.1	44.9
lherz.	PAN3	56.4	0.3	2.3	2.7	1.8	nd	15.3	18.9	2.1	nd	94.0	2.0	0.01	0.1	0.1	0.1	0.8	0.7	0.1	93.9	45.4
lherz.	PAN3	56.1	0.3	1.8	2.2	1.7	nd	16.4	19.7	1.5	nd	96.5	2.0	0.01	0.1	0.1	0.0	0.9	0.8	0.1	94.6	45.0
lherz.	PAN3	55.7	0.5	0.8	1.2	2.0	nd	17.1	21.7	0.7	0.1	94.3	2.0	0.01	0.0	0.0	0.1	0.9	0.8	0.0	94.0	46.1
ecl.	PAN4	55.7	0.4	7.4	nd	6.7	nd	9.8	15.5	4.6	nd	97.9	2.0	0.01	0.3	-	0.2	0.5	0.6	0.3	72.3	45.2
ecl.	PAN4	55.9	nd	7.3	nd	6.9	nd	9.6	15.6	4.7	nd	98.6	2.0	-	0.3	-	0.2	0.5	0.6	0.3	71.3	45.4
ecl.	PAN4	55.5	nd	7.3	nd	7.0	nd	9.8	15.6	4.8	nd	99.9	2.0	-	0.3	-	0.2	0.5	0.6	0.3	71.4	44.8
ecl.	PAN4	55.7	nd	7.3	nd	6.8	0.4	9.7	15.3	4.7	nd	100.4	2.0	-	0.3	-	0.2	0.5	0.6	0.3	71.8	44.9
ecl.	PAN4	55.6	nd	7.3	nd	6.9	nd	9.9	15.5	4.8	nd	99.8	2.0	-	0.3	-	0.2	0.5	0.6	0.3	71.9	44.8
ecl.	PAN4	55.5	nd	7.4	nd	7.0	nd	9.8	15.6	4.8	nd	96.6	2.0	-	0.3	-	0.2	0.5	0.6	0.3	71.2	44.9
ecl.	PAN4	55.8	0.3	7.1	nd	6.6	nd	9.9	15.7	4.6	nd	98.8	2.0	0.01	0.3	-	0.2	0.5	0.6	0.3	72.6	45.3
ecl.	PAN4	55.4	nd	7.3	nd	7.0	nd	9.8	15.6	4.9	nd	96.6	2.0	-	0.3	-	0.2	0.5	0.6	0.3	71.4	44.8
ecl.	PAN4	55.9	nd	7.3	nd	6.7	nd	9.8	15.6	4.7	nd	98.5	2.0	-	0.3	-	0.2	0.5	0.6	0.3	72.3	45.3
ecl.	PAN4	55.2	nd	6.3	nd	6.9	nd	10.4	16.9	4.3	nd	96.4	2.0	-	0.3	-	0.2	0.6	0.7	0.3	72.9	45.9

Suite	Sample	SiO_2	TiO_2	Al_2O_3	Cr_2O_3	FeO	NiO	MgO	CaO	Na_2O	K_2O	total	Si	Ti	Al	Cr	Fe	Mg	Ca	Na	Mg#	Ca#
Clinopyroxene																						
ecl.	PAN4	55.8	0.3	7.2	nd	6.7	nd	9.8	15.6	4.6	nd	99.9	2.0	0.01	0.3	-	0.2	0.5	0.6	0.3	72.2	45.4
ecl.	PAN4	55.9	nd	7.3	nd	6.5	nd	9.8	15.8	4.6	nd	100.2	2.0	-	0.3	-	0.2	0.5	0.6	0.3	72.8	45.6
ecl.	PAN4	55.0	nd	7.2	0.3	6.9	nd	10.0	15.9	4.7	nd	91.6	2.0	-	0.3	0.0	0.2	0.5	0.6	0.3	72.1	45.1
ecl.	PAN4	55.5	nd	7.1	nd	7.4	nd	9.7	15.6	4.7	nd	99.5	2.0	-	0.3	-	0.2	0.5	0.6	0.3	70.1	44.6
ecl.	PAN4	55.4	0.3	7.2	nd	7.2	nd	9.8	15.4	4.7	nd	102.0	2.0	0.01	0.3	-	0.2	0.5	0.6	0.3	70.8	44.5
ecl.	PAN4	55.7	nd	7.2	nd	6.7	nd	9.8	15.8	4.7	nd	100.3	2.0	-	0.3	-	0.2	0.5	0.6	0.3	72.2	45.5
ecl.	PAN4	55.7	0.4	7.3	nd	6.6	nd	9.7	15.5	4.8	nd	101.2	2.0	0.01	0.3	-	0.2	0.5	0.6	0.3	72.3	45.5
ecl.	PAN4	55.5	nd	7.3	nd	7.1	nd	9.8	15.6	4.7	nd	100.2	2.0	-	0.3	-	0.2	0.5	0.6	0.3	71.2	44.9
ecl.	PAN4	55.0	nd	7.0	0.3	7.4	nd	9.9	15.7	4.7	nd	99.6	2.0	-	0.3	0.0	0.2	0.5	0.6	0.3	70.3	44.5
ecl.	PAN4	55.3	0.3	7.3	nd	7.0	nd	9.9	15.4	4.7	nd	101.7	2.0	0.01	0.3	-	0.2	0.5	0.6	0.3	71.6	44.5
ecl.	PAN4	56.0	nd	7.2	nd	6.9	nd	9.8	15.5	4.7	nd	100.3	2.0	-	0.3	-	0.2	0.5	0.6	0.3	71.7	45.0
ecl.	PAN4	55.3	0.3	7.2	nd	6.5	0.4	9.8	15.7	4.8	nd	101.5	2.0	0.01	0.3	-	0.2	0.5	0.6	0.3	72.9	45.6
Olivine																						
lherz.	PAN8	43.4	nd	0.3	nd	8.5	0.4	47.2	0.1	0.2	nd	65.5	1.6	-	0.0	-	0.3	2.6	0.0	0.0	90.9	-
lherz.	PAN8	44.1	nd	0.2	nd	8.5	0.4	46.4	nd	0.3	nd	79.4	1.6	-	0.0	-	0.3	2.5	-	0.0	90.6	-
lherz.	PAN8	45.2	nd	nd	nd	6.5	0.4	47.5	0.1	0.2	nd	95.6	1.6	-	-	-	0.2	2.5	0.0	0.0	92.8	-
	PAN7	44.0	nd	nd	0.1	6.4	0.5	48.8	nd	0.2	0.1	95.2	1.6	-	-	0.0	0.2	2.6	-	0.0	93.1	-
	PAN7	44.0	nd	nd	0.1	7.3	0.5	47.8	nd	0.3	nd	94.1	1.6	-	-	0.0	0.2	2.6	-	0.0	92.1	-
	PAN7	44.6	nd	nd	nd	6.8	0.4	47.9	nd	0.3	nd	94.3	1.6	-	-	-	0.2	2.6	-	0.0	92.6	-
	PAN7	43.9	nd	nd	0.1	6.7	0.4	48.6	0.1	0.2	nd	94.7	1.6	-	-	0.0	0.2	2.6	0.0	0.0	92.8	-
	PAN7	43.1	nd	0.2	0.2	9.5	0.4	46.3	nd	0.3	nd	59.8	1.6	-	0.0	0.0	0.3	2.5	-	0.0	89.7	-
lherz.	PAN1	43.7	nd	nd	nd	8.5	0.3	47.3	nd	0.3	nd	96.6	1.6	-	-	-	0.3	2.6	-	0.0	90.9	-
lherz.	PAN1	44.0	nd	nd	nd	8.1	0.3	47.4	nd	0.3	nd	97.9	1.6	-	-	-	0.2	2.6	-	0.0	91.3	-
lherz.	PAN1	44.7	nd	nd	nd	8.3	0.3	46.3	0.2	0.2	nd	94.1	1.6	-	-	-	0.3	2.5	0.0	0.0	90.8	-
lherz.	PAN1	43.9	nd	nd	nd	8.4	0.3	47.0	nd	0.3	nd	96.1	1.6	-	-	-	0.3	2.5	-	0.0	90.9	-
lherz.	PAN1	43.7	nd	nd	nd	8.8	0.3	47.0	nd	0.2	nd	85.6	1.6	-	-	-	0.3	2.5	-	0.0	90.5	-
lherz.	PAN1	43.9	nd	nd	nd	8.3	0.4	47.2	nd	0.3	nd	95.7	1.6	-	-	-	0.3	2.5	-	0.0	91.0	-
lherz.	PAN1	43.8	nd	nd	nd	8.4	0.3	47.3	nd	0.3	nd	94.7	1.6	-	-	-	0.3	2.6	-	0.0	91.0	-
lherz.	PAN1	43.9	nd	nd	nd	8.6	0.4	46.7	nd	0.3	nd	88.0	1.6	-	-	-	0.3	2.5	-	0.0	90.6	-
Orthopyroxene																						
lherz.	PAN3	63.0	nd	1.7	nd	5.5	0.4	28.7	0.3	0.2	0.2	61.5	2.1	-	0.1	-	0.2	1.4	0.0	0.0	90.3	0.7
lherz.	PAN3	64.1	nd	0.7	nd	5.4	0.4	28.8	0.2	0.2	0.2	59.8	2.2	-	0.0	-	0.2	1.4	0.0	0.0	90.6	0.5
lherz.	PAN3	66.2	nd	1.0	nd	4.1	0.3	27.5	0.3	0.1	0.2	43.8	2.2	-	0.0	-	0.1	1.4	0.0	0.0	92.2	0.6
lherz.	PAN3	60.6	nd	0.6	nd	6.2	0.4	30.8	0.8	0.3	0.3	47.4	2.1	-	0.0	-	0.2	1.6	0.0	0.0	89.8	1.6

sample	PAN2					PAN3					PAN5					PAN6					Peridotitic	
inc. no.	18	24	41	43	ave. (σ)	2	3	12	17	ave. (σ)	8	23	25	28	ave. (σ)	1	4	10	12	ave. (σ)	Brine (±)	Carb. (±)
wt% oxide																						
SiO_2	3.9	6.6	3.8	2.9	4.6 (2.2)	4.6	2.2	2.8	2.9	3.1 (0.7)	8.2	5.0	7.8	8.1	5.8 (2.5)	5.6	2.7	3.3	3.3	4.0 (2.2)	2.2 (0.5)	7.6 (0.4)
TiO_2																					-	-
Al_2O_3	1.3	1.2	0.9	0.6	1.4 (1.4)			0.7	0.7	0.8 (0.6)	6.5			1.1	1.9 (1.9)				1.0	1.3 (0.4)	-	2.5 (1.1)
MgO	14.9	7.8	2.1	9.3	5.7 (3.9)	6.0	2.3	2.8	4.0	3.3 (1.6)	12.4	3.1	6.4	10.8	7.8 (5.6)	11.3	1.2	2.9	2.4	4.6 (3.4)	0.0 (0.7)	14.1 (2.6)
FeO	29.4	18.5	5.4	20.0	12.2 (7.8)	12.6	3.7	6.3	5.6	6.9 (2.5)	30.9	8.0	23.4	29.6	26.8 (14.2)	36.5	5.4	16.0	8.9	16.9 (11.4)	1.4 (2.0)	37.6 (0.7)
CaO	19.9	14.6	2.6	10.5	7.1 (4.8)	7.7	3.4	3.6	3.6	4.9 (2.3)	16.7	5.7	8.4	14.0	12.7 (9.6)	16.4	3.0	8.7	3.2	7.6 (4.9)	0.7 (0.7)	19.9 (1.7)
BaO	6.3	15.1	11.2	15.2	12.0 (6.7)	17.6	15.1	16.6	12.9	17.2 (4.7)	16.5	7.1	7.3	16.4	11.4 (7.3)	21.8	11.7	11.6	12.5	15.7 (4.7)	14.7 (5.3)	16.6 (1.7)
Na_2O	2.2	3.3	4.4	2.7	3.9 (1.7)	4.9	6.0	4.9	4.2	4.6 (0.9)	3.1	13.5	2.9	3.2	5.9 (4.4)	2.5	6.9	4.1	9.3	7.6 (3.4)	10.3 (4.2)	1.6 (0.5)
K_2O	10.2	12.9	34.3	20.0	22.4 (10.7)	23.0	32.3	31.0	34.2	27.9 (5.9)	2.1	29.0	21.1	5.4	12.7 (10.8)	1.4	33.7	28.9	28.4	21.9 (11.3)	34.3 (0.5)	-
P_2O_5																	1.6				-	-
Cl	7.5	14.1	32.8	15.4	21.3 (9.3)	23.6	32.1	29.6	30.6	29.2 (4.3)	1.5	28.6	19.6	4.7	13.1 (10.9)	1.9	33.7	24.6	29.7	23.4 (9.6)	36.5 (11.9)	-
Total	21.2	14.8	12.8	28.3	13.5 (4.9)	6.5	6.2	6.3	6.1	6.1 (2.3)	7.2	7.3	6.6	8.3	7.9 (1.9)	9.7	7.0	10.0	9.0	7.9 (3.6)	-	-
mol. %																						
Si	4.0	7.2	3.8	3.1	5.0 (4.7)	4.7	2.2	2.9	2.9	3.2 (3.2)	9.4	4.7	7.9	9.5	6.1 (3.8)	6.5	2.6	3.3	3.3	4.0 (4.2)	2.1 (0.3)	8.4 (0.7)
Ti																					-	-
Al	0.8	0.8	0.5	0.4	0.9 (1.7)			0.4	0.4	0.5 (1.5)	4.4			0.8	1.2 (1.7)			0.0	0.6	0.8 (0.5)	-	1.6 (0.8)
Mg	23.0	12.7	3.1	15.0	9.1 (12.3)	9.1	3.5	4.3	5.9	4.9 (10.8)	21.1	4.4	9.7	18.8	12.3 (12.6)	19.7	1.8	4.4	3.6	6.8 (10.1)	0.0 (1.5)	23.1 (3.6)
Fe	25.4	16.9	4.5	18.1	11.0 (13.7)	10.7	3.1	5.4	4.7	5.9 (9.7)	29.5	6.4	19.9	28.9	23.6 (17.8)	35.7	4.4	13.5	7.4	14.0 (18.7)	1.1 (2.9)	34.6 (1.8)
Ca	22.1	17.1	2.8	12.2	8.2 (10.8)	8.4	3.7	3.9	3.8	5.3 (11.3)	20.4	5.8	9.2	17.5	14.3 (15.4)	20.5	3.1	9.4	3.4	8.1 (10.3)	0.7 (1.4)	23.4 (1.3)
Ba	2.6	6.5	4.3	6.4	7.3 (5.5)	7.0	6.0	6.7	5.0	6.9 (8.4)	7.4	2.7	2.9	7.5	4.7 (4.3)	10.0	4.5	4.6	4.9	6.1 (3.6)	5.6 (5.6)	7.2 (1.0)
Na	2.2	3.5	4.2	2.8	4.1 (3.6)	4.8	5.9	4.9	4.0	4.6 (4.0)	3.4	12.4	2.9	3.6	6.0 (6.4)	2.8	6.6	4.0	8.9	7.3 (6.4)	9.6 (10.3)	1.7 (0.6)
K	6.7	9.0	21.7	13.8	15.4 (14.4)	14.9	20.8	20.2	21.7	18.2 (17.2)	1.5	17.6	13.7	4.0	8.5 (10.3)	1.0	21.1	18.6	18.0	13.8 (14.2)	21.1 (9.5)	-
P																	2.7				-	-
Cl	13.2	26.2	55.1	28.2	38.9 (33.3)	40.6	54.9	51.4	51.6	50.5 (33.9)	2.9	46.1	33.8	9.3	23.3 (27.7)	3.8	56.0	42.1	50.0	39.2 (32.0)	59.7 (0.3)	-
K/Cl	0.51	0.34	0.39	0.49	0.40 (0.43)	0.37	0.38	0.39	0.42	0.36 (0.51)	0.53	0.38	0.40	0.43	0.37 (0.37)	0.28	0.38	0.44	0.36	0.35 (0.44)	-	-
KNa/Cl	0.68	0.48	0.47	0.59	0.50 (0.54)	0.49	0.49	0.49	0.50	0.45 (0.63)	1.71	0.65	0.49	0.82	0.62 (0.60)	1.03	0.49	0.54	0.54	0.54 (0.64)	-	-
CaFeMg/Cl	5.36	1.79	0.19	1.60	0.73 (1.11)	0.69	0.19	0.26	0.28	0.32 (0.94)	24.46	0.36	1.15	7.01	2.15 (1.65)	20.16	0.17	0.65	0.29	0.74 (1.22)	-	-
Ca/(CaMgFe)	0.31	0.37	0.27	0.27	0.29 (0.29)	0.30	0.36	0.29	0.27	0.33 (0.36)	0.29	0.35	0.24	0.27	0.29 (0.34)	0.27	0.34	0.34	0.24	0.28 (0.26)	-	-

Sample	PAN7					PAN8					PAN4										Eclogitic	
Inc. no.	2	10	12	30	ave. (σ)	3	10	13	19	ave. (σ)	7	8	9	13	14	17	20	23	24	ave. (σ)	Brine (±)	Carb. (±)
wt% oxide																						
SiO_2	7.6	1.7	3.3	2.7	3.5 (1.4)	6.4	2.8	4.5	3.9	4.5 (2.1)	18.9	13.1	22.8	5.9	25.9	11.0	12.3	10.3	13.0	15.1 (6.4)	3.4 (3.4)	39.1 (4.6)
TiO_2						10.0	5.5	9.8	4.6	6.1 (2.5)	1.8							1.6		0.3 (0.6)	-	-
Al_2O_3			0.6	0.9	0.8 (0.1)						1.9	1.0	1.8	1.6	2.8	1.9	1.1	1.3	1.5	1.7 (0.7)	0.7 (0.1)	4.0 (0.2)
MgO	11.0	2.4	3.9	3.0	4.9 (3.1)	11.4	2.8	6.6	4.7	5.5 (4.2)	1.8	1.1	1.7	0.9	1.8	1.1	0.9	1.1	1.8	1.2 (1.0)	0.0 (0.0)	4.3 (0.0)
FeO	31.7	10.6	10.0	19.6	18.9 (13.8)	34.9	5.5	19.3	8.2	13.6 (11.3)	8.6	8.7	10.9	11.6	11.1	11.5	8.2	10.8	11.8	9.8 (3.3)	9.4 (0.4)	12.8 (0.4)
CaO	15.6	5.3	5.2	5.8	9.0 (5.6)	15.1	3.6	8.8	4.8	7.4 (6.2)	5.1	5.1	5.6	3.3	5.8	3.5	3.5	4.2	4.2	4.9 (1.8)	0.6 (0.2)	12.7 (0.3)
BaO	17.6	9.1	12.9	9.9	12.0 (7.1)	17.3	5.6	12.1	9.0	11.9 (5.2)	11.8	16.8	12.2	16.6	11.3	11.5	11.9	17.8	12.1	13.2 (3.4)	11.2 (2.1)	14.3 (2.8)
Na_2O	4.0	19.2	11.3	6.7	9.0 (5.3)	4.8	13.4	4.5	15.0	11.8 (5.5)	3.0	4.1	3.3	3.5	3.0	3.8	4.5	5.5	5.0	4.1 (0.8)	3.6 (0.1)	5.0 (0.1)
K_2O	4.3	17.0	23.5	26.2	19.9 9.2)	5.3	30.0	22.7	30.6	22.4 (9.1)	25.6	23.4	22.1	24.8	22.3	26.9	30.3	24.7	25.1	26.0 (6.9)	37.4 (2.8)	0.0 (4.2)
P_2O_5											3.0	3.2	3.1	1.3	2.3	1.9	2.2	3.5	3.3	2.6 (1.3)	1.2 (0.5)	7.9 (1.5)
Cl	4.2	34.2	28.1	23.6	21.4 (9.6)	7.3	34.6	21.1	26.2	26.6 (11.2)	18.7	22.2	16.5	29.7	14.0	26.2	25.2	19.3	22.0	22.2 (6.6)	32.5 (0.4)	0.0 (0.0)
total	7.8	22.4	20.5	29.3	23.2 (10.1)	5.1	5.1	6.7	5.7	5.1 (1.4)	15.2	14.8	6.2	12.5	4.3	8.6	6.9	5.8	6.2	8.0 (3.8)	-	-
mol. %																						
Si	8.6	1.5	3.2	2.8	3.5 (2.6)	6.2	2.5	4.2	3.6	4.0 (3.6)	20.2	14.2	24.5	6.0	28.1	11.3	12.7	11.5	13.7	15.7 (20.1)	3.4 (3.4)	45.8 (4.4)
Ti						7.3	3.7	6.9	3.2	4.1 (3.2)	1.4							1.3		0.2 (1.5)	-	-
Al			0.3	0.5	0.5 (0.2)						1.2	0.6	1.1	1.0	1.8	1.1	0.7	0.9	0.9	1.0 (1.3)	0.4 (0.0)	2.7 (0.1)
Mg	18.7	3.2	5.7	4.6	7.3 (8.7)	16.4	3.8	9.2	6.4	7.3 (10.7)	2.9	1.8	2.7	1.4	2.9	1.7	1.4	1.8	2.8	1.9 (4.7)	0.0 (0.0)	7.4 (0.2)
Fe	30.2	8.0	8.2	16.8	16.0 (21.5)	28.2	4.1	15.1	6.4	10.2 (16.2)	7.7	7.9	9.8	9.9	10.1	9.8	7.1	10.1	10.4	8.5 (8.7)	7.9 (1.5)	12.5 (0.1)
Ca	19.0	5.1	5.5	6.4	9.7 (11.2)	15.6	3.5	8.9	4.7	7.1 (11.3)	5.8	5.9	6.5	3.6	6.8	3.8	3.9	5.0	4.7	5.5 (5.9)	0.7 (0.1)	16.0 (0.0)
Ba	7.9	3.2	4.9	4.0	4.8 (5.2)	6.6	1.9	4.4	3.3	4.2 (3.5)	4.9	7.1	5.2	6.6	4.8	4.6	4.8	7.8	5.0	5.4 (4.2)	4.4 (2.1)	6.6 (1.5)
Na	4.4	16.8	10.7	6.7	8.8 (9.6)	4.5	11.5	4.1	13.5	10.2 (9.1)	3.1	4.3	3.4	3.5	3.2	3.8	4.5	5.9	5.1	4.1 (2.6)	3.5 (1.0)	5.7 (0.3)
K	3.1	9.8	14.7	17.2	12.8 (10.9)	3.3	17.0	13.6	18.0	12.8 (9.9)	17.5	16.1	15.2	16.1	15.5	17.6	19.9	17.6	16.8	17.3 (13.9)	24.0 (8.0)	0.0 (3.2)
P											1.4	1.5	1.4	0.6	1.1	0.8	1.0	1.7	1.5	1.1 (1.7)	0.4 (0.1)	3.2 (0.5)
Cl	8.1	52.3	46.7	41.1	36.6 (30.2)	11.9	52.1	33.6	40.9	40.3 (32.5)	33.9	40.7	30.1	51.4	25.8	45.5	44.1	36.5	39.2	39.2 (35.2)	55.4 (12.6)	0.0 (0.0)
K/Cl	0.39	0.19	0.31	0.42	0.35 (0.36)	0.27	0.33	0.40	0.44	0.32 (0.31)	0.51	0.40	0.50	0.31	0.60	0.39	0.45	0.48	0.43	0.44 (0.40)		
KNa/Cl	0.93	0.51	0.54	0.58	0.59 (0.68)	0.65	0.55	0.53	0.77	0.57 (0.58)	0.61	0.50	0.62	0.38	0.72	0.47	0.55	0.64	0.56	0.55 (0.47)		
CaFeMg/Cl	8.37	0.31	0.41	0.68	0.90 (1.37)	5.05	0.22	0.99	0.43	0.61 (1.17)	0.48	0.38	0.63	0.29	0.77	0.34	0.28	0.46	0.46	0.41 (0.55)		
Ca/(CaMgFe)	0.28	0.31	0.28	0.23	0.29 (0.27)	0.26	0.31	0.27	0.27	0.29 (0.30)	0.36	0.38	0.34	0.24	0.34	0.25	0.31	0.30	0.26	0.35 (0.31)		